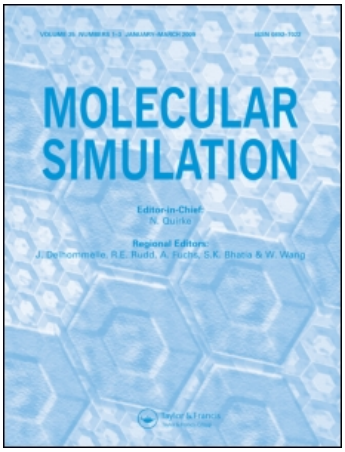

Molecular Simulation
Publication details, including instructions for authors and subscription information:
http://www.informaworld.com/smpp/title~content=t713644482

Vapor-liquid equilibria and thermophysical behavior of the SPC-HW model for heavy water

A. A. ChIalvo[a]; J. Horita[a]
[a] Chemical Sciences Division, Aqueous Chemistry and Geochemistry Group, Oak Ridge National Laboratory, Oak Ridge, TN, USA

To cite this Article ChIalvo, A. A. and Horita, J.(2005) 'Vapor-liquid equilibria and thermophysical behavior of the SPC-HW model for heavy water', Molecular Simulation, 31: 14, 1035 — 1042
To link to this Article: DOI: 10.1080/08927020500412508
URL: http://dx.doi.org/10.1080/08927020500412508

Molecular Simulation, Vol. 31, No. 14–15, 15–30 December 2005, 1035–1042

Vapor–liquid equilibria and thermophysical behavior of the SPC-HW model for heavy water

A. A. CHIALVO* and J. HORITA

Chemical Sciences Division, Aqueous Chemistry and Geochemistry Group, Oak Ridge National Laboratory, Oak Ridge, TN 37831-6110, USA

(Received October 2005; in final form October 2005)

The vapor–liquid coexistence curve of the simple point charge heavy-water model (SPC-HW), [*J. Chem. Phys.*, *114*, 8064–8067 (2001)] is determined by Gibbs Ensemble Monte-Carlo (GEMC) simulation. The estimated critical conditions of the model based on the Wegner-type expansion for the order parameters and the rectilinear diameter are $\rho_c = 0.300$ g/cc, $T_c = 661$ K and $P_c = 156$ bars. The dielectric constant determined by isothermal–isochoric molecular dynamics is underpredicted along the coexistence curve by 29–44% in comparison with the experimental values. The analysis of the orthobaric temperature dependence of the system microstructure, in terms of the three site–site radial distribution functions, indicates that the first coordination numbers for the oxygen–oxygen and the oxygen–deuterium interactions are $\sim 4.3 \pm 0.1$ and $\sim 1.9 \pm 0.1$ at $T = 300$ K, and decrease by 15 and 55%, respectively, at criticality. The dipole–dipole correlation functions show that the orientational order in heavy water is quickly lost beyond the first oxygen–oxygen coordination shell. The model's second virial coefficient is determined by Monte-Carlo integration and used to aid the interpretation of the predicted phase equilibrium results.

Keywords: Heavy water; Vapor–liquid equilibria; SPC-HW model; Gibbs Ensemble Monte-Carlo; Second virial coefficient

1. Introduction

Heavy water (D_2O) has been of great interest in several disciplines due to its peculiar properties including its high moderating effect and small neutron-capture cross section making D_2O specially advantageous as a moderator in nuclear reactors [1,2], its large difference in coherent scattering amplitude with respect to that of H_2O that makes the neutron diffraction with isotopic substitution (NDIS) possible [3], its cytotoxic and cytostatic activity against human cancer cell that renders D_2O as a potential anticancer agent [4], and its ability to increase thermal-neutron flux penetration and dose homogeneity of epithermal neutron beams for boron neutron capture therapy [5].

Even though heavy water is "almost" identical to light water [6], the replacement of light by heavy water affects the microstructure of water and macromolecules in solution [7–14], as well as the related time-dependent properties [15–17]. The stronger deuterium bonds in D_2O than their counterparts in H_2O, resulting from the heavier deuterium atom that lowers the zero-point vibrational energy of the intermolecular modes [18], translates into a slight increase in the D_2O structure around itself [19,20]. The immediate consequence is the possibility of stronger (weaker) solvation of hydrophilic (hydrophobic) solutes in D_2O than in H_2O environments [21–23].

Despite the alleged similarity between several properties of D_2O and H_2O (e.g. see table 1 of Némethy and Scheraga [6]), these two fluids behave so distinctly in other important aspects that the origin and their consequences require an explicit molecular-based analysis. In fact, the notion of negligible conformational and thermophysical effects on macromolecular aqueous solutions, resulting from the substitution of H_2O by D_2O, has recently been challenged by Raman scattering photon correlation spectroscopy, small angle neutron scattering and NMR measurements [24,25].

Moreover, the common simulation practice to deal with aqueous deuterated environments in classical simulations, i.e. by doubling the hydrogen mass in the involved water models [26–32], can only provide some insight into the H_2O/D_2O mass effect on the dynamical properties, however, this trick obviously cannot offer any hint on the actual isotopic effect on the equilibrium properties. In fact, within the framework of classical

*Corresponding author. Fax: +1-865-574-4961. Email: chialvoaa@ornl.gov

Molecular Simulation
ISSN 0892-7022 print/ISSN 1029-0435 online © 2005 Taylor & Francis
http://www.tandf.co.uk/journals
DOI: 10.1080/08927020500412508

statistical mechanics, the equilibrium properties depend only on the strength of the intermolecular forces (i.e. they are mass independent [33]).

Suitable ways to tackle the simulation analysis of the effect of the H_2O/D_2O substitution on the equilibrium and dynamic behavior of aqueous systems involve typically quantum approaches based on *ab initio* formalisms [34], path integrals formalisms of quantum statistical mechanics [35], the Feynman–Hibbs variational approach [36] and combinations of the others [37]. Currently, *ab initio* methods are computationally too expensive to be implemented for the study of the above-mentioned systems of interest. In that sense, path integrals methods are better suited to that end, since they lead to the definition of an effective potential that can be used within the context of classical molecular simulations [38,39].

Yet, the H_2O/D_2O substitution can also be studied entirely in terms of effective potentials, beyond the Feynman–Hibbs [36] and Wigner–Kirkwood [40,41] perturbations approaches, by describing independently either H_2O or D_2O. This approach was recently used by Grigera [42] who proposed an effective pair potential for D_2O, the simple point charge heavy-water model (SPC-HW), to describe and reproduce some properties of D_2O at ambient conditions. As for the case of the majority of the effective potentials whose parameterization have been performed at ambient conditions, the lingering question is whether the resulting model is able to describe accurately the fluid behavior at conditions away from those of its parameterization, as well as to predict other relevant properties. Regardless of the answer to the proposed question, this inquiry usually becomes the starting point of a broader analysis that usually leads to improvements of the current model and/or the rethinking of its modeling strategy [43,44].

Our goal here is to characterize the behavior SPC-HW model for heavy water, by determining its vapor–liquid phase coexistence curve, the corresponding dielectric constant, microstructure and second virial coefficient to test the adequacy of the model prior to its application in other studies. Our interest in a classical model for heavy water stems from the lack of thermophysical properties for beyond 800 K and 1000 bars, needed in our studies of the pressure effect on the reduced partition function ratio for hydrogen isotopes in water [45] and its implications on the high-pressure isotopic partitioning in Earth and other planets.

For that purpose, in Section 2 we describe the model and the two simulation methods used in this study. In Section 3, we discuss the simulation results, including the determination of the vapor–liquid coexistence curve and the resulting critical conditions, the orthobaric temperature dependences of the dielectric constant and microstructure, as well as the model's second virial coefficient by invoking the corresponding experimental results whenever available. Finally, in Section 4, we wrap up this work with some final remarks and outlook.

2. Potential model and simulation methodology

The SPC-HW model [42] involves the same geometry and Lennard–Jones parameters as in the SPC-E water model [46] but scaled (augmented) electrostatic charges to adjust the predicted D_2O properties resulting in an effective dipole moment $\mu = 2.41$ D, i.e. about 3% larger than that for the SPC-E water model. In fact, the charge in the oxygen site is $q_O = -2q_D = -0.87e$ so that the polarization contribution $E_{pol} = (\mu - \mu_{isol})^2/2\alpha$ (where $\alpha = 1.444$ Å^3 is assumed to be equal to the molecular polarizability of H_2O) becomes equal to 6.286 kJ/mol, i.e. ~20% larger than that for the SPC-E water model.

For the study of the thermodynamic behavior of the SPC-HW model we apply two different, though complementary, simulation methodologies. First, we run Gibbs Ensemble Monte-Carlo (GEMC) simulations [47] to determine the vapor–liquid coexistence curve predicted by the model. Then, we run isochoric–isothermal molecular dynamics (NVT-MD) simulations along particular orthobaric states, as predicted by the GEMC, to determine the behavior of the corresponding dielectric constant and microstructure.

All NVT-MD simulations involved 500 molecules, whose Euler–Newton equations of motion were integrated using a 5th and 4th order (for translational and rotational degrees of freedom, respectively) Gear's predictor–corrector algorithm [48] with a time-step of 1.0 fs. The rotational degrees of freedom were described by Evans and Murad's quaternion formalism [49], and the isothermal condition was achieved using a couple of independent Nosé thermostats [50] for the rotational and translational degrees of freedom.

All interactions were truncated at a center-to-center cutoff distance of $3.0\sigma_{OO}$, while the long range electrostatic interactions were calculated using an Ewald summation with a convergence parameter $\alpha \approx 5.6/L$ where L is the length of the cubic simulation box, and a maximum k in the reciprocal space such that $k^2 \leq 27$. After an equilibration period of 20 ps, all runs spanned 1 ns for the determination of the dielectric constant, during which the three site–site radial distribution functions and the dipole–dipole correlations functions were also extracted.

For the constant volume GEMC simulation we applied the standard methodology [51] involving $N = 500$ molecules. Each run comprised about 3500 equilibration cycles for both phases (the first run starting from random configurations and the subsequent ones from dumped configurations from previous runs), where each cycle comprises $2.22N$ randomly chosen move attempts, including N center of mass translations, N molecular rotations around randomly chosen molecular axes, $0.02N$ phase volume changes and $0.2N$ molecular transfers between phases with a 50% average acceptance ratio for the first two types of moves. The equilibrations are followed by the production runs comprising 8000–10,000 cycles (i.e. 9.6–12 millions configurations),

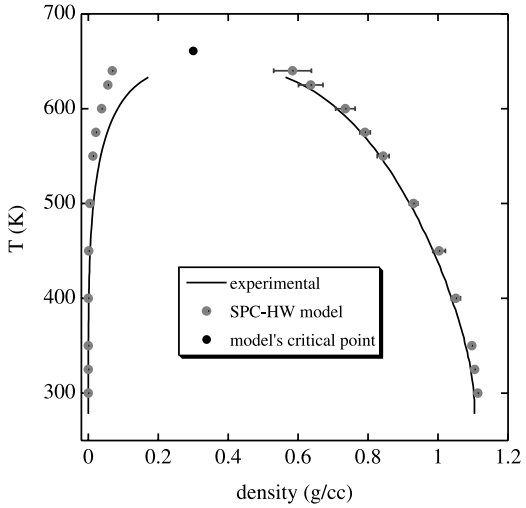

Figure 1. Vapor–liquid equilibrium of the SPC-HW as predicted by GEMC simulation in comparison with the actual phase envelope of D_2O [62].

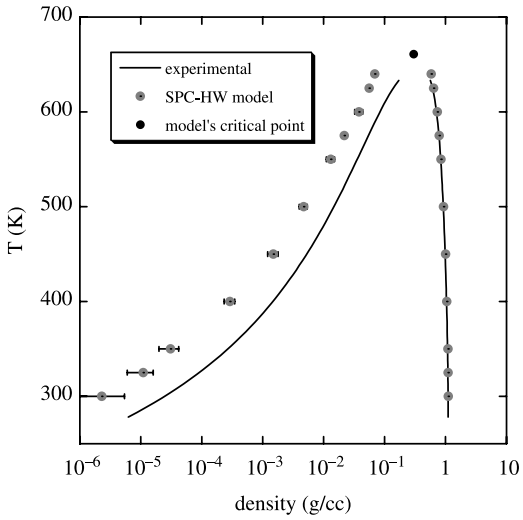

Figure 2. Same as in figure 1 but using a logarithmic scale for the densities to disclose clearly the inaccuracy of the vapor phase predictions.

divided in 10 blocks of 500 cycles (∼0.6 million configurations) each, from which the block averages are obtained [52].

3. Simulation results and discussion

3.1 Vapor–liquid equilibrium (VLE) and critical conditions

In figure 1, we display the resulting VLE behavior of the SPC-HW model. It becomes clear that the SPC-HW is able to predict reasonably well the vapor–liquid phase behavior, even though its performance deteriorates quickly as it approaches the critical region, especially for the vapor phase. In fact, the deficiency in the prediction of the vapor phase density is clearly revealed by plotting the VLE in a linear-log plot as shown in figure 2.

While the model provides an accurate temperature dependence of the orthobaric density for the liquid phase, the corresponding vapor phase density is underestimated. This behavior is not unexpected for non-polarizable rigid models, i.e. in that to account for the sizable polarization effects in the liquid-like environments the force-field parameters of these models are fitted to properties of the liquid phases. Consequently, the fitted electrostatic charges are augmented over those corresponding to the isolated (gas phase) molecule, and the resulting models are usually unable to predict accurately and simultaneously the properties of the liquid- and vapor-like media [53]. An alternative way to detect this deficiency is by plotting the temperature dependence of the predicted vapor pressure, as depicted in figure 3, where the SPC-HW underpredicts the vapor pressure over the entire range, with a Clausius–Clapeyron slope ∼20% smaller than that for real D_2O.

For the estimation of the model critical point based on the simulated orthobaric curve, we invoke the Wegner expansion [54,55], i.e.

$$\rho_l - \rho_v = A_0|1 - T/T_c|^{\beta} + A_1|1 - T/T_c|^{\beta+\Delta} + A_2|1 - T/T_c|^{\beta+2\Delta}\ldots \quad (1)$$

where T_c is the critical temperature, A_i are the amplitude coefficients, β is the critical exponent and Δ is the so-called gap exponent. According to the Renormalization Group Theory, $\beta = 0.325$ and $\Delta = 0.5$ for the VLE case, and therefore, we can in principle determine the critical temperature and exponent from the regression of equation (1). Likewise, the critical density can be determined from the expansion of the rectilinear diameter [56], i.e.

$$\rho_l + \rho_v = 2\rho_c + B_1|1 - T/T_c|^{\phi} + B_2|1 - T/T_c| + B_3|1 - T/T_c|^{\phi+\Delta}\ldots \quad (2)$$

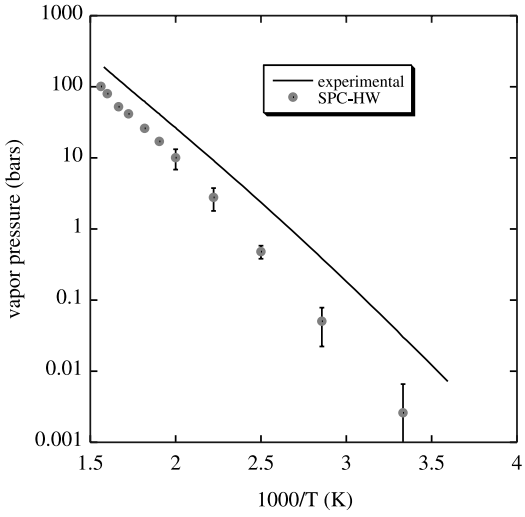

Figure 3. Comparison between the temperature dependence of the vapor pressure predicted by the SPC-HW model and that corresponding to D_2O [62].

where $\phi = 1 - \alpha$ and α is the critical exponent of the weak singularity ascribed to the heat capacity. However, here we proceed by combining the two expressions and keeping the leading terms [57,58], to obtain our working expression,

$$\rho_{\pm} = \rho_c + B_2|1 - T/T_c| \pm 0.5A_0|1 - T/T_c|^{\beta_e} \qquad (3)$$

where the plus (minus) sign refers to the liquid (vapor) phase, and the subscript "e" at β highlights the fact that this parameter is considered as an effective exponent. The effective critical exponent, first defined by Verschaffelt [59] as,

$$\beta_e = \partial \ln(\rho_l - \rho_v)/\partial \ln|1 - T/T_c| \qquad (4)$$

is a sensitive measure of the shape of the orthobaric curve. Therefore, the regression of the VLE data from the GEMC simulation according to equation (3), by using a non-linear least squares method, allows us to determine the five parameters including ρ_c, T_c, β_e. Finally, to estimate the corresponding critical pressure, we fit the temperature dependence of the vapor pressure to the Clausius–Clapeyron expression [60], i.e. $\ln P(T) = a + b/T$ so that $P_c = \exp(a + b/T_c)$.

From the non-linear regression of the coexistence data we obtain $\beta_e \cong 0.330$, $\rho_c = 0.300$ g/cc, $T_c = 661$ K and consequently, $P_c = 156$ bars in comparison with the theoretical value of $\beta = 0.325$ and the experimental values of $\rho_c = 0.356$ g/cc, $T_c = 643.9$ K and $P_c = 217$ bars, respectively [61,62].

3.2 Microstructure of heavy water along the coexistence curve

In figures 4–6, we present the orthobaric temperature dependence of the three site–site radial distribution functions, i.e. $g_{OO}(r)$, $g_{OD}(r)$ and $g_{DD}(r)$, for the liquid branch of the coexistence curve. The obvious, though not surprising, feature of these functions is their similarity to those for the SPC-E water model [63]. For example, at $T = 300$ K the $g_{OO}(r)$ exhibits a first peak at ~ 2.78 Å, corresponding to a coordination $n_O^O(r_s = 3.3\,\text{Å}) = 4\pi\rho_O \int_0^{r_s} g_{OO}(r) r^2 dr$ of $\sim 4.3 \pm 0.1$, followed by a shallow valley at ~ 3.3 Å and the second peak at 4.5 Å. The second peak corresponds to the second coordination number $n_O^O(r_u = 5.6\,\text{Å}, \quad r_l = 3.3\,\text{Å}) = 4\pi\rho_O \int_{r_l}^{r_u} g_{OO}(r)\, r^2 dr$ of ~ 20.0 additional D_2O molecules, whose location is known as the signature of the tetrahedral hydrogen-bond configuration of water [64]. In this regard, the $g_{OD}(r)$ presents two well defined peaks at ~ 1.74 and ~ 3.24 Å separated by a deep valley at ~ 2.38 Å, which translates into a first coordination number $n_O^D(r_s = 2.38\,\text{Å}) = 4\pi\rho_D \int_0^{r_s} g_{OD}(r)\, r^2 dr$ of $\sim 1.9 \pm 0.1$

As the orthobaric temperature increases the strength of the first peak of $g_{OD}(r)$ decreases and widens as expected due to the simultaneous density decrease. This widening translates into an approximately 1.0 Å-shift of the location of the first valley from ~ 3.3 Å at $T = 300$ K to ~ 4.3 Å at criticality, with a similar shift for the corresponding second peak, i.e. from ~ 4.5 to ~ 5.5 Å (figure 4). Note however, that the first coordination number $n_O^O(r_s)$ is only reduced by less than 15%, i.e. to $\sim 3.8 \pm 0.1$, while the corresponding $n_O^D(r_s)$ decreases drastically by more than 55% from $\sim 1.9 \pm 0.1$ at $T = 300$ K to $\sim 0.8 \pm 0.1$ at criticality. This behavior indicates that, even after a decrease of density by a factor of ~ 3.78, the system at criticality is still able to keep almost one deuterium-bonded molecule per D_2O molecule in a similar fashion as per light water [65]. Obviously, in the vicinity of the system critical point the three site–site radial distribution functions develop long-range tails governed by the increasing correlation length that goes as the system isothermal compressibility, i.e. it diverges at criticality [66].

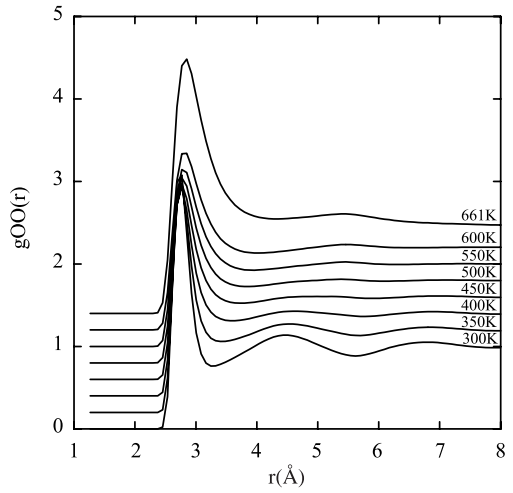

Figure 4. Orthobaric temperature dependence of the radial distribution function for the O–O interactions. For clarity all curves are shifted by 0.2 from one another.

Two other subtle but clear changes are observed in the behavior of $g_{OD}(r)$ and $g_{DD}(r)$ along the coexistence curve. The location of the first two peaks of $g_{OD}(r)$ shifts

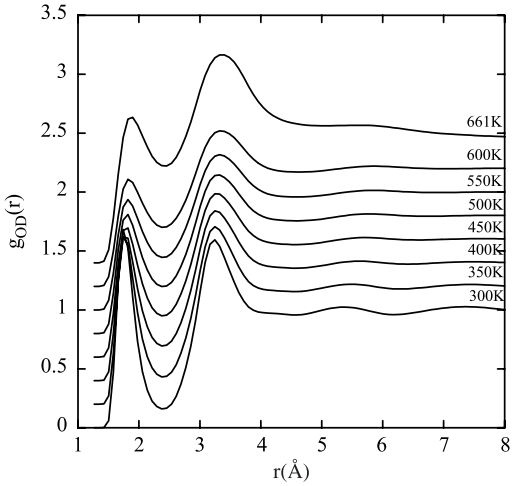

Figure 5. Orthobaric temperature dependence of the radial distribution function for the O–D interactions. For clarity all curves are shifted by 0.2 from one another.

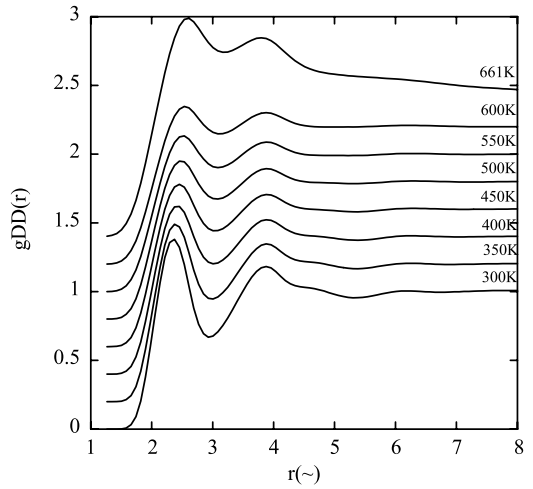

Figure 6. Orthobaric temperature dependence of the radial distribution function for the D–D interactions. For clarity all curves are shifted by 0.2 from one another.

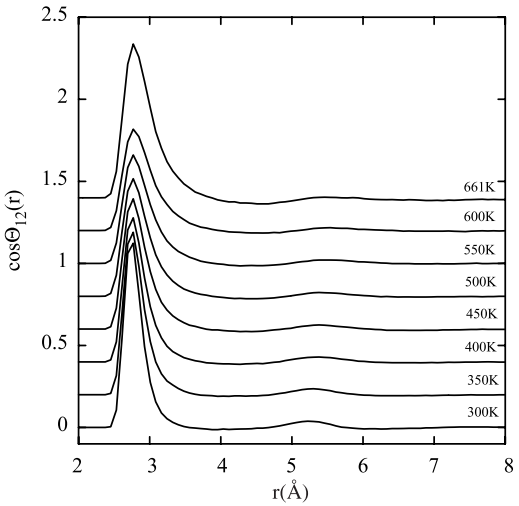

Figure 7. Orthobaric temperature dependence of the dipole–dipole correlation function $G_1(r)$. For clarity all curves are shifted by 0.2 from one another.

by ~ 0.15 and ~ 0.07 Å, respectively, as the orthobaric temperatures increases from ambient to criticality, indicative of a small stretching of the hydrogen bond with decreasing orthobaric density. Similar shift is experienced by the first two peaks of $g_{\mathrm{DD}}(r)$, where the shifts are ~ 0.23 and ~ 0.07 Å, respectively. In both cases the first peak becomes smaller and the corresponding first valley becomes shallower as the orthobaric liquid phase density decreases.

In order to further interpret the resulting structural behavior we determine the lth order dipole–dipole correlations, i.e.

$$G_{\mathrm{l}}(r) = \frac{V}{4\pi r^2}\langle \delta(r - r_{12})\mathrm{R_l}(\cos\Theta_{12})\rangle \qquad (5)$$

where $\langle \ldots \rangle$ denotes an ensemble average, $\mathrm{P_l}(x)$ is the normalized Legendre polynomial and Θ_{12} is the angle formed by the dipole moments of molecules 1 and 2 [67]. Note that the volume integral of $G_1(r)$ is associated with the dielectric constant of the system through the fluctuation of the total dipole moment of the system, i.e.

$$\frac{\langle M^2\rangle}{N\mu^2} = 1 + 4\pi\rho\int_0^\infty G_1(r)r^2\mathrm{d}r \qquad (6)$$

The orthobaric temperature dependence of the first-order dipole–dipole correlation functions is given in figure 7. The obvious feature of these functions is the positive correlation represented by the first peak which indicates that the D_2O molecules within the first solvation shell prefer the parallel alignment, i.e. the dipole moments of two neighboring molecules are pointing into the same direction. Moreover, this picture indicates that the orientational (dipolar) order is almost completely lost beyond the first nearest neighbors. In fact, $G_1(r)$ exhibits a minute bump within the region $5.20\,\text{Å} < r < 5.48\,\text{Å}$, i.e. a remnant of orientational correlation that is associated with the disappearing of the third peak of $g_{\mathrm{OD}}(r)$ (figure 5) and corresponding valley of $g_{\mathrm{DD}}(r)$ (figure 6).

3.3 Dielectric behavior along the coexistence curve

Since we are dealing with a non-polarizable model under periodic boundary conditions, involving an Ewald summation approach to the electrostatic interactions, we apply the following working expression for the dielectric constant [68],

$$\varepsilon = \frac{1 + 2\varepsilon_{\mathrm{RF}}\left[1 + 4\pi(\langle M^2\rangle - \langle M\rangle^2)/3kTV\right]}{1 + 2\varepsilon_{\mathrm{RF}} - 4\pi(\langle M^2\rangle - \langle M\rangle^2)/3kTV} \qquad (7)$$

where $\varepsilon_{\mathrm{RF}}$ is the dielectric permittivity surrounding the replicated simulation box (reaction field), $M = \left|\sum_i \mu_\iota\right|$ with $|\mu_i| = 2.41$ D, and $\langle \ldots \rangle$ indicates a time average over trajectories in the phase space of the system. For simulation purposes the $\varepsilon_{\mathrm{RF}}$ values were taken from the tabulated experimental data [69].

In figure 8, we present the simulation results for the dielectric constant of the SPC-HW along the coexistence curve, in comparison with the corresponding experimental data [69]. Obviously, the SPC-HW is able to capture the dielectric behavior of D_2O, within about 29–44% of the experimental values for the liquid phase between ambient to the critical temperature. A similar behavior is also observed for the coexisting vapor phase, which is just an indication of the poor description of the two-body interactions by the SPC-HW, better highlighted by the behavior of its second virial coefficient as discussed in the next section.

3.4 Second virial coefficient

To aid the characterization and interpretation of the model we also determine its second virial coefficient, i.e. the 6-dimensional integral over the Boltzmann factor by a Monte-Carlo numerical integration [70]. The relative orientation of the pair of SPC-HW molecules are specified by the polar coordinates (r, θ, φ) and the three Euler angles (ω_1, ω_2, ω_3) of the second molecule while keeping the first

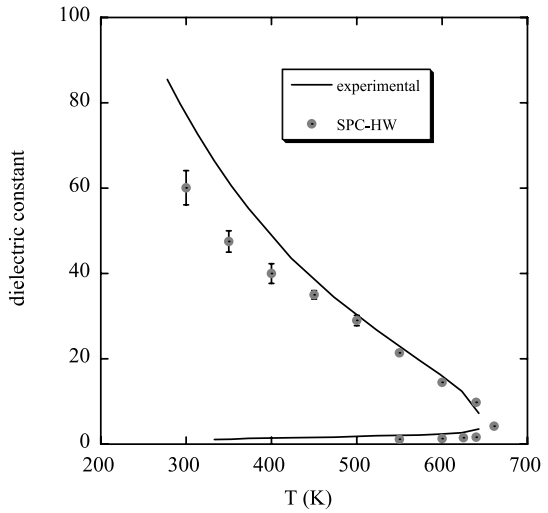

Figure 8. Orthobaric temperature dependence of the dielectric constant of the SPC-HW as predicted by NVT-MD simulations in comparison with the experimental data of D_2O [69].

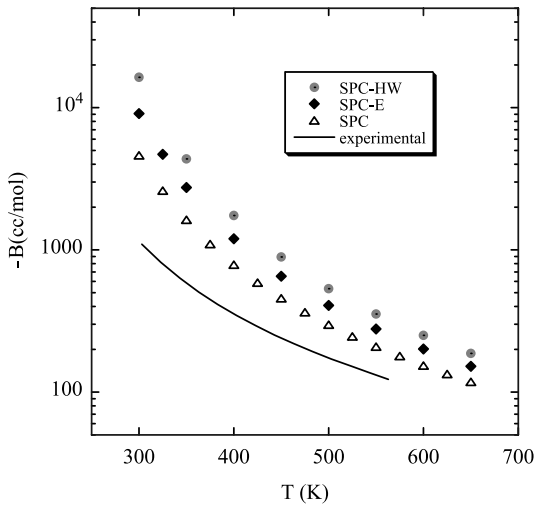

Figure 9. Temperature dependence of the negative value of the second virial coefficient as predicted by the SPC-HW model in comparison with those of the SPC and SPC-E models and the actual behavior for D_2O [72].

molecule fixed at the origin. Thus,

$$B(T) = -\frac{N_A}{16\pi^2}\int_0^\infty r^2 dr \int_0^{2\pi} d\varphi \int_0^\pi \sin\theta\, d\theta \int_0^{2\pi} d\omega_1 \int_0^\pi \sin\omega_2\, d\omega_2 \int_0^\pi \{\exp[-U(r,\theta,\varphi,\omega)/kT] - 1\} d\omega_3 \quad (8)$$

where N_A is Avogadro's number. For numerical purposes the radial integration was divided into three intervals, namely, $0 \le r \le 2.5$ Å for which the (hard sphere) analytical solution is available since $\exp[-U(r, \theta, \varphi, \omega)/kT] \approx 0$, 2.5 Å $\le r \le$ 6.0 Å where the Monte-Carlo integration is actually performed through the evaluation of the function for $\sim 10^6$ random configurations, and $r \ge 6.0$ Å where $U(r, \theta, \varphi, \omega)$ is approximated by a dipole–dipole interaction with a dipole moment $\mu = 2.41$ D for which an analytical solution is also available [71].

In figure 9, we display the comparison between the predicted values for the second virial coefficient of the SPC-HW model and the corresponding experimental data [72]. Note that the SPC-HW model underpredicts $B(T)$ of D_2O in a similar way as the SPC and SPC-E models do it for H_2O. In fact, since these three models share the same geometry and Lennard–Jones parameters, we expect that equation (8) predicted a more negative value of $B(T)$ with an increasing molecular dipole moment (i.e. 2.27, 2.35 and 2.14 D for SPC, SPC-E and SPC-HW, respectively) as clearly depicted in figure 9, because this is the leading term in the multipole expansion of the long-range electrostatic interactions.

Because $B(T)$ is determined independent of either NVT-MD or GEMC simulations, its calculation provides an opportunity to test the consistency of the GEMC simulation results. For that purpose we use the low-pressure portion of the vapor-phase branch of the coexistence curve, where we can assume with confidence the following virial approximation [73],

$$\frac{P(T)}{\rho_v kT} \cong 1 + B(T)\rho_v \quad (9)$$

Thus, we can re-calculate the coexistence vapor density ρ_v in terms of the GEMC's predicted $P(T)$ and the independently calculated $B(T)$ (equation (8)), by solving the quadratic equation and taking the physically meaningful root, i.e.

$$\rho_v = [2B(T)]^{-1}\left[1 - \sqrt{1 + \frac{4P(T)B(T)}{kT}}\right] \quad (10)$$

Figure 10, where we show the comparison between ρ_v from the GEMC simulations and the corresponding values from the virial expansion (equation (10)), suggests that

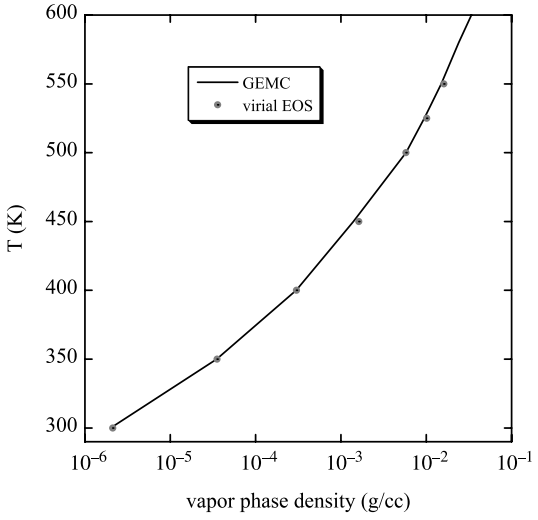

Figure 10. Comparison between the orthobaric vapor densities predicted by the GEMC simulations and the low-pressure virial equation using the calculated $B(T)$ for the SPC-HW model.

$B(T)$ and the vapor coexisting densities from the GEMC simulations are internally consistent.

4. Final remarks

The typical way to assess the adequacy of an intermolecular potential is by testing its ability to describe accurately the properties used in the adjustment of the model parameters away from the conditions of optimization, and to equally predict at any state conditions properties other than those used in the parameterization. Towards that end, in this contribution we have first determined by GEMC simulation the vapor–liquid coexistence curve for the SPC-HW model of D_2O including its critical conditions, and then studied the orthobaric temperature dependences of its dielectric constant and microstructure. In addition, we have calculated the second virial coefficient and used it to test the consistency of the orthobaric vapor phase densities.

The second virial coefficient calculation clearly indicates the failure of this member of the SPC family of models to capture the actual pairwise intermolecular interactions of D_2O, and therefore, the inaccurate prediction of the orthobaric vapor phase densities. This is a defect common to most rigid non-polarizable water models whose effective electrostatics must effectively account for the substantial polarization in the condensed phase through augmented (over those of the actual isolated molecular pair) coulombic charges [74]. For the same reason, it is not surprising to find a reasonable agreement between the predicted and the actual temperature dependence of the orthobaric liquid phase densities, as previously seen for the SPC-E model (e.g. figure 1 of Errington and Panagiotopoulos work [75]), while the corresponding enthalpy of vaporization is overpredicted by both models (see figure 11 for the SPC-HW and figure 5 of Boulougouris *et al.* [76] for the SPC-E model).

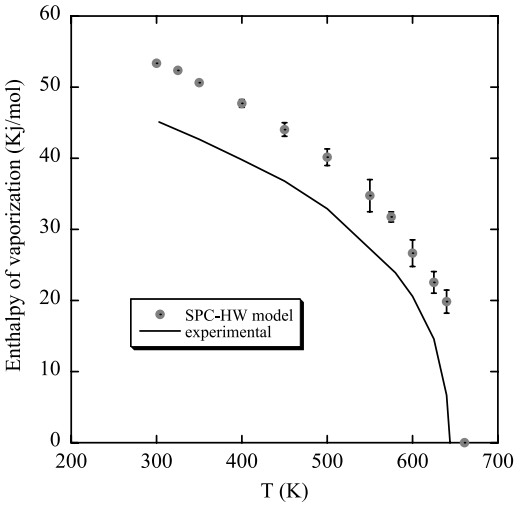

Figure 11. Enthalpy of vaporization of the SPC-HW as predicted by GEMC simulation in comparison with the experimental values for D_2O [62].

In summary, the SPC-HW model is the first attempt (at least that we are aware of) to describe the properties of D_2O by an effective pair potential. Because this model is a spinoff of the SPC family of H_2O models, it also suffers from most of the same defects, some of them exacerbated by the larger effective dipole moment. While this similarity might be the model's curse, it might also be its advantageous feature as to become the best reference for any promising model improvement.

Acknowledgements

This research was sponsored by the Division of Chemical Sciences, Geosciences, and Biosciences, Office of Basic Energy Sciences under contract number DE-AC05-00OR22725 with Oak Ridge National Laboratory, managed and operated by UT-Battelle, LLC.

References

[1] Y. Kowata, N. Fukumura. Neutron absorber effect on coolant void reactivity in a pressure-tube-type heavy-water reactor. *Nucl. Sci. Eng.*, **108**(3), 308 (1991).
[2] J.A. Ayres, C.A. Trilling. Heavy water and organic fluids as neutron moderator and reflector materials. *Nucl. Eng. Des.*, **14**(3), 363 (1970).
[3] J.C. Dore, M. Garawi, M.-C. Bellissent-Funel. Neutron diffraction studies of the structure of water at ambient temperatures, revisited. A review of past developments and currents problems. *Mol. Phys.*, **102**, 2015 (2004).
[4] H. Takeda, *et al.* Mechanisms of cytotoxic effects of heavy water (deuterium oxide: D_2O) on cancer cells. *Anti-Cancer Drugs*, **9**(8), 715 (1998).
[5] Y. Sakurai, T. Kobayashi. The medical-irradiation characteristics for neutron capture therapy at the heavy water neutron irradiation facility of Kyoto University research reactor. *Med. Phys.*, **29**(10), 2328 (2002).
[6] G. Némethy, H.A. Scheraga. Structure of water and hydrophobic bonding in proteins. IV. The Thermodynamic properties of liquid deuterion oxide. *J. Chem. Phys.*, **41**, 680 (1964).
[7] P. Sobrado, P.F. Fitzpatrick. Solvent and primary deuterium isotope effects show that lactate CH and OH bond cleavages are concerted in Y254F flavocytochrome b(2), consistent with a hydride transfer mechanism. *Biochemistry*, **42**(51), 15208 (2003).
[8] R.A. Tinsley, D.A. Harris, N.G. Walter. Significant kinetic solvent isotope effects in folding of the catalytic RNA from the hepatitis delta virus. *J. Am. Chem. Soc.*, **125**(46), 13972 (2003).
[9] V. Najdanovic-Visak, *et al.* Pressure, isotope, and water co-solvent effects in liquid–liquid equilibria of (ionic liquid plus alcohol) systems. *J. Phys. Chem. B*, **107**(46), 12797 (2003).
[10] P. Cioni, G.B. Strambini. Effect of heavy water on protein flexibility. *Biophys. J.*, **82**(6), 3246 (2002).
[11] P. Bernal, J. McCluan. Apparent molar volumes and adiabatic compressibilities of crown ethers and glymes in H_2O and D_2O at 25 degrees C. *J. Solution Chem.*, **30**(2), 119 (2001).
[12] V.K. Abrosimov, *et al.* Solvent isotope effects on the solubility of argon and pair interactions in aqueous solution of hexamethylenetetramine. *Russ. Chem. Bull.*, **49**(8), 1383 (2000).
[13] D.B. Northrop, Y.K. Cho. Effects of high pressure on solvent isotope effects of yeast alcohol dehydrogenase. *Biophys. J.*, **79**(3), 1621 (2000).
[14] J.H. Tian, *et al.* The role of the medium in solvent isotope effects on serine protease action. *Can. J. Chem.-Revue Canadienne De Chimie*, **77**(5–6), 781 (1999).
[15] M. Freda, *et al.* Influence of hydration on dynamical properties of reverse micelles. *J. Non-Cryst. Solids*, **307**, 874 (2002).
[16] D. Pant, N.E. Levinger. Polar solvation dynamics of H_2O and D_2O at the surface of zirconia nanoparticles. *J. Phys. Chem. B*, **103**(37), 7846 (1999).
[17] C.K.J. Grunwald, C. Wöll. In deuterated water the unspecific adsorption of proteins is significanttly slowed down: results of an SPR study using model organic surfaces. *Langmuir*, **21**, 9017 (2005).

[18] S. Scheiner, M. Cuma. Relative stability of hydrogen and deuterium bonds. *J. Am. Chem. Soc.*, **118**(6), 1511 (1996).

[19] B. Tomberli, *et al.* Isotopic quantum effects in water structure measured with high energy photon diffraction. *J. Phys.: Condens. Matter*, **12**(12), 2597 (2000).

[20] L.H. de la Pena, P.G. Kusalik. Quantum effects in light and heavy liquid water: a rigid-body centroid molecular dynamics study. *J. Chem. Phys.*, **121**(12), 5992 (2004).

[21] F. Bonnete, D. Madern, G. Zaccai. Stability against denaturation mechanisms in halophilic malate-dehydrogenase adapt to solvent conditions. *J. Mol. Biol.*, **244**(4), 436 (1994).

[22] G.C. Kresheck, H. Schneide, H.A. Scheraga. Effect of D_2O on thermal stability of proteins. Thermodynamic parameters for transfer of model compounds from H_2O to D_2O. *J. Phys. Chem.*, **69**(9), 3132 (1965).

[23] P. Sasisanker, *et al.* Solvation properties and stability of ribonuclease A in normal and deuterated water studied by dielectric relaxation and differential scanning/pressure perturbation calorimetry. *Phys. Chem. Chem. Phys.*, **6**(8), 1899 (1905).

[24] C. Branca, *et al.* Criticism to light–heavy water substitution in structural studies of macromolecular aqueous solutions. *Physica B*, **270**(3–4), 350 (1999).

[25] C. Branca, *et al.* Can the isotopic H <- > D substitution affect the conformational properties of polymeric aqueous solutions? The poly(ethylene oxide)–water case. *J. Phys.: Condens. Matter*, **11**(32), 6079 (1999).

[26] R. Guzzi, C. Arcangeli, A.R. Bizzarri. A molecular dynamics simulation study of the solvent isotope effect on copper plastocyanin. *Biophys. Chem.*, **82**(1), 9 (1999).

[27] P.J. Steinbach, R.J. Loncharich, B.R. Brooks. The effects of environment and hydration on protein dynamics—a simulation study of myoglobin. *Chem. Phys.*, **158**(2–3), 383 (1991).

[28] X. Yu, D.M. Leitner. Thermal transport coefficients for liquid and glassy water computed from a harmonic aqueous glass. *J. Chem. Phys.*, 123 (2005).

[29] P.H. Nguyen, G. Stock. Nonequilibrium molecular-dynamics study of the vibrational energy relaxation of peptides in water. *J. Chem. Phys.*, **119**(21), 11350 (2003).

[30] C.P. Lawrence, J.L. Skinner. Flexible TIP4P model for molecular dynamics simulation of liquid water. *Chem. Phys. Lett.*, **372**(5–6), 842 (2003).

[31] L.R. Martins, M.S. Skaf, B.M. Ladanyi. Solvation dynamics at the water/zirconia interface: molecular dynamics simulations. *J. Phys. Chem. B*, **108**(51), 19687 (2004).

[32] J. Ropp, *et al.* Rotational motion in liquid water is anisotropic: a nuclear magnetic resonance and molecular dynamics simulation study. *J. Am. Chem. Soc.*, **123**(33), 8047 (2001).

[33] D.A. McQuarrie. *Statistical mechanics*, Harper and Row, New York (1976).

[34] B. Chen *et al.* Hydrogen bonding in water. *Phys. Rev. Lett.*, **91**(21), (2003).

[35] R.P. Feynman. *Statistical mechanics. A set of lectures*, Westview Press, Boulder (1972).

[36] R.P. Feynman, A.R. Hibbs. *Quantum mechanics and path integrals*, McGraw-Hill, New York (1965).

[37] M.E. Tuckerman. Ab Initio *molecular dynamics and* Ab Initio *path integrals, in quantum simulations of complex many-body systems. from theory to algorithms*, D.M.J. Grotendorst, A. Muramatsu (Eds), NIC, Jülich (2002).

[38] B. Guillot, Y. Guissani. Hydrogen-bonding in light and heavy water under normal and extreme conditions. *Fluid Phase Equilib.*, **151**, 19 (1998).

[39] L.M. Sese. Feynman–Hibbs quantum effective potentials for Monte-Carlo simulations of liquid neon. *Mol. Phys.*, **78**(5), 1167 (1993).

[40] J.G. Kirkwood. Quantum statistics of almost classical assemblies. *Phys. Rev.*, **44**, 31 (1933).

[41] E. Wigner. On the quantum correction for thermodynamic equilibrium. *Phys. Rev.*, **40**, 749 (1932).

[42] J.R. Grigera. An effective pair potential for heavy water. *J. Chem. Phys.*, **114**, 8064 (2001).

[43] B. Guillot. A reappraisal of what we have learnt during three decades of computer simulations on water. *J. Mol. Liq.*, **101**(1–3), 219 (2002).

[44] A. Baranyai, A. Bartok, A.A. Chialvo. Computer simulation of the 13 crystalline phases of ice. *J. Chem. Phys.*, **123**(5) (2005).

[45] V.B. Polyakov, J. Horita, D.R. Cole. Pressure effects on the reduced partition function ratio for hydrogen isotopes in water. *Geochemica et Cosmochimica Acta*, (2005).

[46] H.J.C. Berendsen, J.R. Grigera, T.P. Straatsma. The missing term in effective pair potentials. *J. Phys. Chem.*, **91**, 6269 (1987).

[47] A.Z. Panagiotopoulos. Direct determination of phase coexistence properties of fluids by Monte-Carlo simulation in a new ensemble. *Mol. Phys.*, **61**, 813 (1987).

[48] C.W. Gear. *The numerical integration of ordinary differential equations of various orders*, Argonne National Laboratory, Chicago (1966).

[49] D.J. Evans, S. Murad. Singularity free algorithm for molecular dynamics simulation of rigid polyatomics. *Mol. Phys.*, **34**, 327 (1977).

[50] S. Nosé. A unified formulation of the constant temperature molecular dynamics methods. *J. Chem. Phys.*, **81**, 511 (1984).

[51] A.Z. Panagiotopoulos. Adsorption and capillary condensation of fluids in cylindrical pores by Monte-Carlo simulation in the Gibbs ensemble. *Mol. Phys.*, **62**, 701 (1987).

[52] H. Flyvbjerg, H.G. Petersen. Error-estimates on averages of correlated data. *J. Chem. Phys.*, **91**, 461 (1989).

[53] A.A. Chialvo, P.T. Cummings. *Molecular-based modeling of water and aqueous solutions at supercritical conditions, in advances in chemical physics*, S.A. Rice (Ed.), pp. 115–205, Wiley, New York (1999).

[54] F.J. Wegner. Corrections to scaling laws. *Phys. Rev. B*, **5**(11), 4529 (1972).

[55] J.V. Sengers, J.M.H. Levelt Sengers. *Critical phenomena in classical fluids, in progress in liquid physics*, C.A. Croxton (Ed.), pp. 103–174, Wiley, Chichester (1978).

[56] M. Ley-Koo, M.S. Green. Consequences of the renormalization-group for the thermodynamics of fluids near the critical-point. *Phys. Rev. A*, **23**(5), 2650 (1981).

[57] D.G. Green, *et al.* Vapor–liquid and liquid–liquid phase-equilibria of mixtures containing square-well molecules by Gibbs ensemble Monte-Carlo simulation. *J. Chem. Phys.*, **101**(4), 3190 (1994).

[58] L. Vega, *et al.* Phase-equilibria and critical-behavior of square-well fluids of variable width by Gibbs ensemble Monte-Carlo simulation. *J. Chem. Phys.*, **96**(3), 2296 (1992).

[59] R.R. Singh, K.S. Pitzer. Relationships in the approach to criticality in fluids, including systematic differences between vapor–liquid and liquid–liquid systems. *J. Chem. Phys.*, **90**, 5742 (1989).

[60] J.S. Rowlinson, F.L. Swinton. *Liquids and liquid mixtures*, 3rd ed., Butterworth, London (1982).

[61] J.M.H. Levelt Sengers, *et al.* Assessment of critical parameter values for H_2O and D_2O. *J. Phys. Chem. Ref. Data*, **14**(1), 193 (1985).

[62] J. Kestin, *et al.* Thermo-physical properties of fluid D_2O. *J. Phys. Chem. Ref. Data*, **13**(2), 601 (1984).

[63] Y. Guissani, B.J. Guillot. A computer simulation study of the liquid–vapor coexistence curve of water. *J. Chem. Phys.*, **98**, 8221 (1993).

[64] A. Ben-Naim. *Water and aqueous solutions*, Plenum Press, New York (1974).

[65] A.A. Chialvo, P.T. Cummings. Microstructure of ambient and supercritical water. A direct comparison between simulation and neutron scattering experiments. *J. Phys. Chem.*, **100**, 1309 (1996).

[66] J.V. Sengers, J.M.H. Levelt Sengers. Thermodynamics behavior of fluids near the critical point. *Ann. Rev. Phys. Chem.*, **37**, 189 (1986).

[67] J.P. Hansen, I.R. McDonald. *Theory of simple liquids*, 2nd ed., Academic Press, New York (1986).

[68] S.W. de Leeuw, J.W. Perram, E.R. Smith. Simulation of electrostatic systems in periodic boundary conditions III. Further theory and applications. *Proc. R. Soc. London*, **A388**, 177 (1983).

[69] Y.M. Lukashov, V.N. Shcherbakov, V.V. Savenko. An experimental investigation of the dielectric constant of heavy water at the saturation line. *Therm. Eng.*, **26**, 728 (1979).

[70] F. Sokolic, Y. Guissani, G. Baranovic. Intermolecular pair potentials and the second virial coefficient of suphur dioxide vapor. *Chem. Phys. Lett.*, **131**, 513 (1986).

[71] J.O. Hirschfelder, C.F. Curtiss, R.B. Bird. *Molecular theory of gases and liquids*, Wiley, New York (1954).

[72] P.G. Hill, R.D.C. Macmillan. Virial equations for light and heavy-water. *Ind. Eng. Chem. Res.*, **27**(5), 874 (1988).

[73] H.C. Van Ness, M.M. Abbott. *Classical thermodynamics of nonelectrolyte solutions*, McGraw Hill, New York (1982).

[74] A. Baranyai, A. Bartok, A.A. Chialvo. *J. Mol. Liq.*, (2005).

[75] J.R. Errington, A.Z. Panagiotopoulos. A fixed point charge model for water optimized for the vapor–liquid coexistence properties. *J. Phys. Chem. B*, **102**, 7470 (1998).

[76] G.C. Boulougouris, I.G. Economou, D.N. Theodorou. Engineering a molecular model for water phase equilibrium over a wide temperature range. *J. Phys. Chem. B*, **102**, 1029 (1998).